

An efficient and low-cost method to create high-density nitrogen-vacancy centers in CVD diamond for sensing applications.

Prem Bahadur Karki,¹ Rupak Timalisina,² Mohammadjavad Dowran,² Ayodimeji E. Aregbesola,¹ Abdelghani Laraoui,^{2,3*} and Kapildeb Ambal^{1†}

¹Department of Mathematics, Statistics, and Physics, Wichita State University, 1845 Fairmount St. Wichita, KS 67260, United States of America

²Department of Mechanical & Materials Engineering, University of Nebraska-Lincoln, 900 N 16th St. W342 NH. Lincoln, NE 68588, United States of America

³Department of Physics and Astronomy and the Nebraska Center for Materials and Nanoscience, University of Nebraska-Lincoln, 855 N 16th St, Lincoln, Nebraska 68588, USA

*[†]Author to whom correspondence should be addressed, email:

*alaraoui2@unl.edu, [†]Kapildeb.ambal@wichita.edu

I. Abstract

The negatively charged Nitrogen-Vacancy (NV⁻) center in diamond is one of the most versatile and robust quantum sensors suitable for quantum technologies, including magnetic field and temperature sensors. For precision sensing applications, densely packed NV⁻ centers within a small volume are preferable due to benefiting from $1/\sqrt{N}$ sensitivity enhancement (N is the number of sensing NV centers) and efficient excitation of NV centers. However, methods for quickly and efficiently forming high concentrations of NV⁻ centers are in development stage. We report an efficient, low-cost method for creating high-density NV⁻ centers production from a relatively low nitrogen concentration based on high-energy photons from Ar⁺ plasma. This study was done on type-IIa, single crystal, CVD-grown diamond substrates with an as-grown nitrogen concentration of 1 ppm. We estimate an NV⁻ density of ~ 0.57 ppm (57%) distributed homogeneously over 200 μm deep from the diamond surface facing the plasma source based on optically detected magnetic resonance and fluorescence confocal microscopy measurements. The created NV⁻s have a spin-lattice relaxation time (T_1) of 5 ms and a spin-spin coherence time (T_2) of 4 μs . We measure a DC magnetic field sensitivity of ~ 104 nT Hz^{-1/2}, an AC magnetic field sensitivity of ~ 0.12 pT Hz^{-1/2}, and demonstrate real-time magnetic field sensing at a rate over 10 mT s⁻¹ using an active sample volume of 0.2 μm^3 .

II. Introduction

The negatively charged nitrogen-vacancy (NV⁻) centers are one of the leading solid state-based quantum platforms [1], enabling diverse quantum applications, including spin-qubit for quantum information processing [2–5], quantum memory [6–8], and quantum sensing [9] for many physical quantities including magnetic fields [10–17], electric fields [18–21], and temperature [22–24]. For potential commercial sensing applications where nanoscale spatial resolution is not required, ensemble NV⁻s are preferred. The key requirements for high-sensitive ensemble-based sensing applications are high NV⁻ concentrations within small volumes while preserving long spin coherence time. The high concentrations are favored for precision magnetometry due to improved signal-to-noise and sensitivity from $1/\sqrt{N}$ enhancement [9,25]. For example, the sensitivity to detect a constant magnetic field with NV⁻ centers scales with $1/\sqrt{N_{\text{NV}}}$ where N_{NV} is the number of NV⁻ centers from which the fluorescence signal is

collected [26]. The densely packed or small sample volume is necessary to efficiently excite NV^- centers using on-chip laser and microwave excitation [27].

Several existing techniques are available for creating high-density NV^- centers > 10 ppm ($1 \text{ ppm} = 1.76 \times 10^{17} \text{ cm}^{-3}$ in diamond) [28]. The most popular ones are; (1) implanting high doses (~ 100 ppm) of nitrogen (N) with subsequent annealing [29–31] and (2) electron irradiation or implantation of He^+ ions on a diamond substrate containing high-concentration of nitrogen (N) impurities (~ 100 ppm) followed by subsequent annealing [32,33]. Nevertheless, the final concentration of NV^- s still depends on many factors like annealing temperature, cleaning procedures, substrate characteristics, and the N to NV^- conversion yield (typically $< 10\%$) [34]. Recently, progress was made to increase the production yield by more than 30% by optimizing the process (e.g., the electron irradiation dose) [35]. However, $> 70\%$ of the implanted/doped nitrogen atoms are present in the substrate as substitutional nitrogen, known as P_1 paramagnetic centers [36,37] or neutral nitrogen-vacancy (NV^0) centers [1]. These excesses of nitrogen unavoidably lead to decreased NV^- center spin coherence properties by orders of magnitude [36–38], thus degrading the sensitivity [25]. Also, a large implantation or electron irradiation dose creates undesired defects and local graphitization of the diamond crystal, which could be beyond repair via the thermal annealing process [39,40]. These unwanted defects decrease spin coherence times T_2^* and T_2 that impact the overall sensitivity. Therefore, developing low-cost and highly efficient methods in creating high-density NV^- centers from low-concentration nitrogen in the diamond crystal is essential to increase the number of NV^- centers for many scientific and commercial applications such as the fabrication of brighter nanodiamonds for biomedical applications [12,22,33,41].

This work focuses on a quick and cost-effective method of creating high-density NV^- centers in type-IIa chemical vapor deposition (CVD)-grown diamond substrates with as-grown nitrogen concentration of 1 ppm by using high-energy photons from Ar^+ plasma. Based on optically detected magnetic resonance (ODMR) and fluorescence confocal microscopy measurements, we estimate the density of newly created $\text{NV}^- \sim 0.57$ ppm ($> 50\%$ of conversion yield), distributed homogeneously over $200 \mu\text{m}$ deep from the diamond surface facing the plasma source. The created NV^- centers exhibit a spin-lattice relaxation time (T_1) of 5 ± 0.2 ms and a spin-spin coherence time (T_2) of $4 \pm 0.5 \mu\text{s}$. We estimate a shot noise-limited DC magnetic field sensitivity of $\sim 104 \text{ nT Hz}^{-1/2}$ an AC magnetic field sensitivity of $\sim 0.12 \text{ pT Hz}^{-1/2}$ respectively over an active sample volume of $0.2 \mu\text{m}^3$, and demonstrate a real-time AC magnetic field sensing with a frequency of up to 90 Hz using the same active sample volume.

III. Experimental methods and discussion

The NV^- center is a solid-state spin sensor in a diamond crystal formed by substituting a carbon atom with a nitrogen atom and a vacancy adjacent to it [1] (inset of **Fig. 1b**). This type of nitrogen-vacancy center is known as the neutral NV^0 center. If the neutral NV center captures an extra electron, it forms a negatively charged NV^- center that can be photoionized to NV^0 with laser or voltage excitations [42,43]. The NV^- center, a spin-1 system, is used for emerging quantum applications, including quantum sensing [9]. The diamond substrates used for this work are single crystal CVD-grown type-IIa diamonds (element six part# 145-500-0055) doped with ~ 1 ppm ($1.76 \times 10^{17} \text{ cm}^{-3}$) of nitrogen (N) throughout the substrate during the growth process. The substrates (labeled 1 and 2) were first cleaned in a tri-acid mixture (1 H_2SO_4 : 1 HNO_3 : 1 HClO_4) [44] for two hours at 200°C to remove polishing-related graphitization, followed by rinsing with deionized (DI) water or Isopropyl Alcohol (IPA) and finally drying using compressed nitrogen gas. The dry

substrates were then exposed to Argon (Ar^+) plasma by using Trion Minilock-Phantom III Inductively Coupled Plasma (ICP) Reactive Ion Etching (RIE) system for 30 s (**Fig. 1(a)**). The plasma process was performed with ICP power at 200 W, RIE power at 50 W, Ar gas flow at 5 sccm, and the ICP-RIE chamber pressure at 10 mTorr. After the plasma exposure, the diamonds were cleaned with the tri-acid mixture for two hours at 200 °C. The dry substrates were then annealed under vacuum (10^{-8} Torr) at 1100 °C for two hours with another subsequent triacid cleaning [31,41]. The clean and dry substrates were then used for optical and spin characterization. We discuss below the mechanisms of NV^- creation using high-energy photons from Ar^+ plasma.

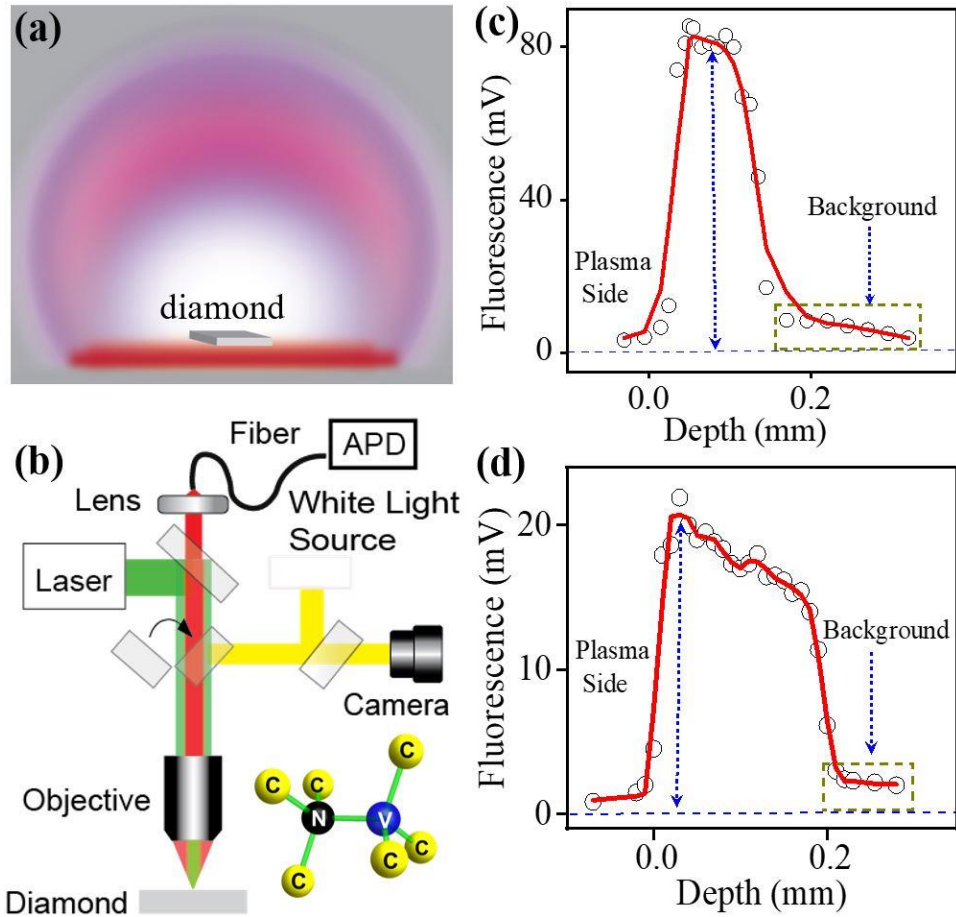


Figure 1. (a) Representation of the process for making a high-density NV^- layer using Ar^+ plasma. (b) schematic of the custom-made confocal optical microscope used to characterize the high-density NV^- centers. Inset of (b) an NV center in a diamond lattice. The distribution of the created NV^- centers as a function of the depth from the side facing the plasma measured on 0.25 mm (c, substrate 1) and 0.5 mm (d, substrate 2) thick diamonds prepared with the same conditions.

The NV^- center is a deep bandgap defect located near the mid-gap within the 5.6 eV bandgap of the diamond crystal [1]. NV^- formation needs three processes: substitutional nitrogen atom, adjacent vacancy, and electron capture. There are two well-established NV^- creation methods: (1) implantation of nitrogen (^{14}N or ^{15}N) ions followed by high-temperature annealing [45], and (2) doping the diamond crystal with N during the growth process and create vacancies by helium ion (He^+) implantation [32,33] or electron irradiation [34,46] followed by subsequent high-

temperature annealing. In both methods, the implantation/irradiation of N/He ions creates a high density of vacancies due to the broken bonds/dangling bonds. During the high-temperature annealing process, these vacancies position themselves next to substitutional nitrogen atoms forming the NV^0 center [1]. When NV^0 captures an extra electron, they become NV^- . Since the diamond has a large bandgap and NV centers are located near the middle of the bandgap, the thermal energy is insufficient to excite electrons from the valence band to the conduction band to be captured. These difficulties lead to poor yield in N-to- NV^- formation. However, electron irradiation creates broken bonds along with extra electrons, improving NV^- formation efficiency [34,45].

High energy and above bandgap photons generated from the Ar⁺ plasma were used to create dangling bonds in SiO₂ [47–49]. The energy of Ar⁺ in the plasma is very low, and the depth of the created NV^- center is more than 200 μm from the surface facing the plasma. Therefore, it is conclusive that the enhancement of NV^- formation is primarily due to high-energy photons from Ar⁺ plasma [50–52]. We hypothesize that the high energy and above bandgap photons from Ar⁺ plasma could have two effects: (i) Direct absorption of UV photons inducing vacancies such as broken bonds/dangling bonds [53]. (ii) When the diamond absorbs a UV photon, it creates a shower of electrons (because the photon energy is much larger than the diamond band gap) [54]. These electrons could travel through the conduction band of the diamond and recapture. Therefore, we assume that the high-energy photons would have similar effects as electron irradiation, creating vacancies and supplying electrons for recapturing. The formation of dangling bonds will create more NV centers from doped N^0/P_1 centers, similar to electron irradiation [34,46]. The excited extra electrons in the conduction band could be captured to form NV^- centers [54].

Optical Characterization.

The fluorescence properties of the diamond substrates were investigated using a custom-built confocal fluorescence microscope [14,55] (**Fig. 1b**) consisting of a green laser (532 nm) for optical excitation of NV^- centers, a permanent magnet (up to 100 mT) to apply a magnetic field for ODMR measurements, a 100x microscope objective with a numerical aperture of 0.8 NA to focus light on the diamond substrate, and fluorescence collection optics including 650 nm edge pass filter, focusing lens, 9/125 single-mode fiber, single photon counter modules (SPCM) used for confocal imaging and spin measurements in **Fig. 2** and **Fig. 3**, and avalanche photodetector (APD) used for measurements in **Fig. 1** and **Fig. 4**.

The diamond substrate is excited with a green (532 nm) laser, and the fluorescence is measured at different depths from the surface facing the plasma, **Figs. 1c, 1d**. We repeat the process to several locations and different substrates thicknesses. The measurement results from two of the representative CVD diamond substrates of thicknesses, 0.25 mm (substrate 1) and 0.5 mm (substrate 2) are shown in **Fig. 1c** and **Fig. 1d**. at a green laser power of 20 mW and 5 mW, respectively. The fluorescence intensity in both diamonds is an order of magnitude higher for the surface facing the Ar⁺ plasma than the other side, which has only background fluorescence coming from the as-grown NV^- centers (< 0.1 ppm). The newly created NV^- s are uniformly distributed over a depth of 150-200 μm depending on the substrate thickness, as shown in **Fig. 1c** and **Fig. 1d**.

To estimate the spatial distribution of the Ar⁺ plasma-created NV^- centers, we performed fluorescence imaging on the surfaces of substrate 2 facing plasma (**Fig. 2a**) at a green laser power of 0.5 mW. **Fig. 2b** shows the line cut profile (dashed line) taken on **Fig. 2a**. It is conclusive that the Ar⁺ plasma created NV^- centers are uniformly distributed. We compare the fluorescence intensity from the newly created ensemble NV^- centers in substrate 1 with the one collected from

an electronic grade (EL) diamond with single NV⁻ centers (created by ion beam implantation of ¹⁵N ions at a dose of $5 \times 10^9 \text{ cm}^{-2}$ and energy of 30 keV) by using the confocal microscope under similar experimental conditions (at saturation). Since our SPCM saturates at a count rate of 10 Mc/s corresponding to a laser power of 3 mW, we used an APD to detect the fluorescence of the plasma-created NV⁻s. In **Fig. 2c**, we plot the fluorescence of substrate 1 as a function of green laser power by converting the APD detected voltage (mV) to counts per second (c/s) and found a photon count rate of 400 Mc/s at saturation ($> 30 \text{ mW}$). Based on single NV⁻ measurements (maximum count rate of 0.02 Mc/s at saturation) on the EL implanted diamond (inset of **Fig. 2d**), we estimate that the side facing Ar⁺ in substrate 1 contains $> 20,000 \text{ NV}^-$ centers over the active volume of $0.2 \mu\text{m}^3$, which translates to an NV⁻ density of $\sim 10^{17} \text{ cm}^{-3}$ ($= 0.57 \text{ ppm}$). To confirm that the detected fluorescence comes from NV⁻ centers, we performed fluorescence vs wavelength measurements on the side of substrate 2 facing Ar⁺ plasma by using spectrometer TRIAX 320 (Horiba), **Fig. 2d**. The observed spectrum consists of a typical NV⁻ curve with high fluorescence in the wavelength range of 650- 760 nm with zero phonon line (ZPL) peaks for NV⁰ and NV⁻ at 574 and 637, nm respectively [1].

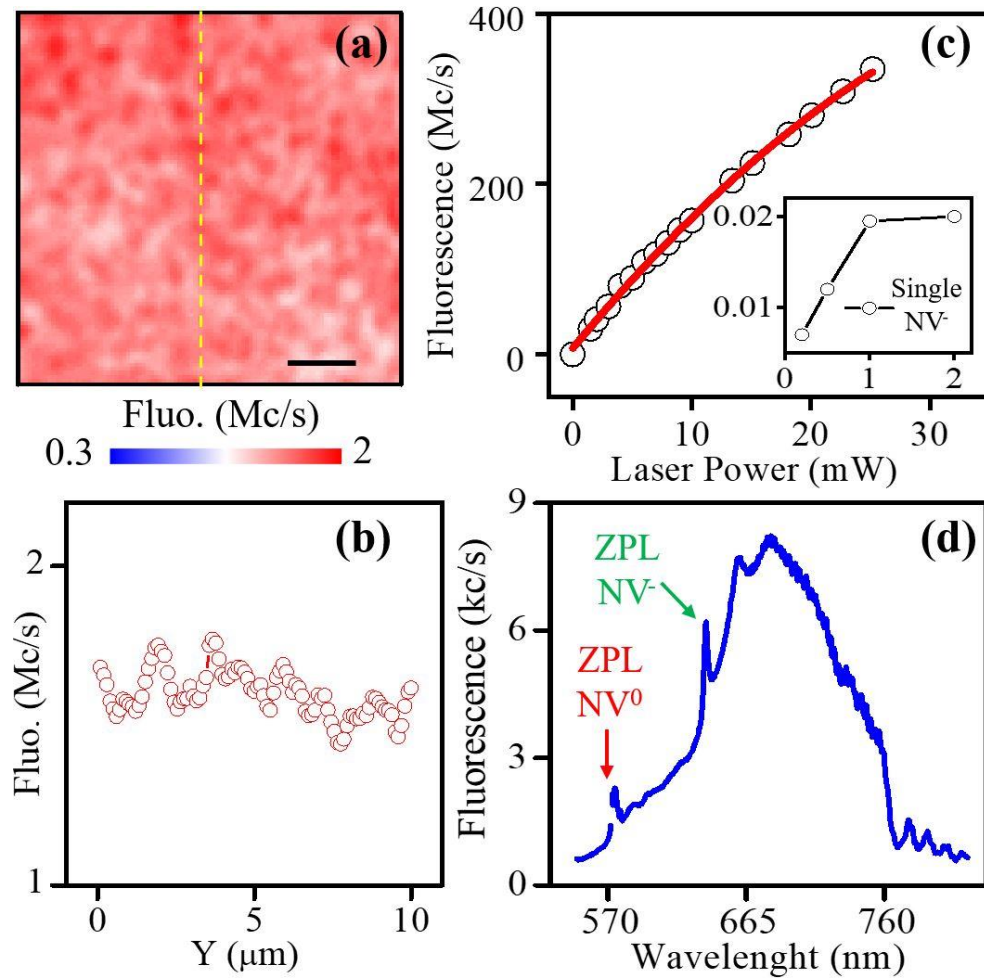


Figure 2. Optical characterization of the Ar⁺ plasma photon irradiated diamond substrates. Fluorescence image of the surface facing the Ar⁺ plasma (a). (b) Vertical line cut of fluorescence spatial profile taken across the dashed lines in (a). (c) The fluorescence of substrate 1 was detected by APD as a function of green laser power. Inset of (c) fluorescence intensity of EL diamond with single NV⁻ centers as a function

of green laser power (20 Kc/s at a laser power of 2 mW). **(d)** Fluorescence spectrum acquired on the surface facing the plasma of substrate 2. Scale bar in **(a)** is 2 μm .

Spin-characterization.

The NV^- center-based sensing application requires narrow resonance linewidth and sufficiently long coherence and relaxation time. The spin-resonance properties of the Ar^+ plasma created high-density NV^- are scrutinized using well-established electron spin resonance measurement methods [14,15,56]. **Fig. 3** shows the outcome of the measurements on substrate 1 performed using the custom-built confocal microscope with SPCM modules and at an applied magnetic field of 8.6 mT applied along [111] orientation of the (100) diamond and at laser power of 1 mW. We discuss the ODMR measurements in detail below.

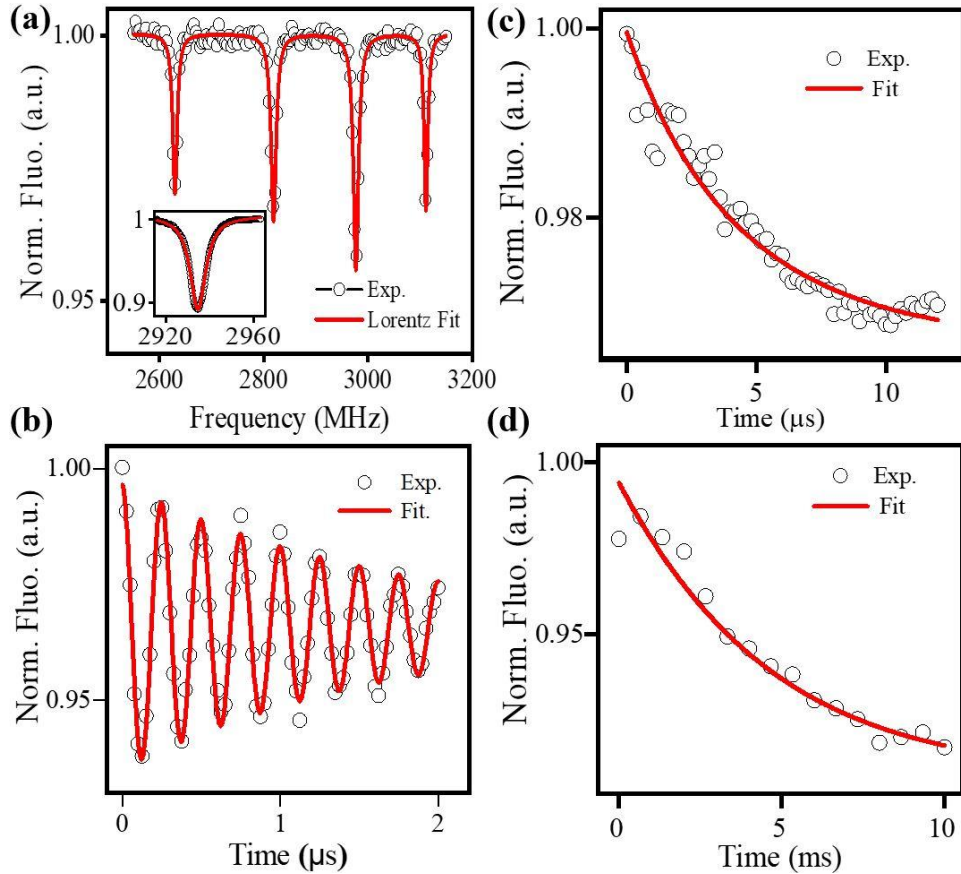


Figure 3. **(a)** CW-ODMR spectrum measured (scattered open circles) at an applied field of 8.6 mT. The solid line curve in **(a)** is Lorentzian fits for the NV ODMR peaks. Insert in **(a)** is the cw-ODMR spectra acquired at 2.3 mT field with optimized laser and MW parameters. **(b)** Rabi-nutation measurement which shows the fluorescence intensity (scattered open circles) vs the duration of applied MW pulse at MW frequency of 2629 MHz and a magnetic field of 8.6 mT. The solid line curve is a fit to the experimental data (see the main text). **(c)** Normalized measured (scattered open circles) fluorescence intensity vs echo time between p pulses fitted (solid line) with an exponential decay function with a decay = T_2 . **(d)** Normalized measured (scattered open circles) fluorescence intensity vs time, fitted with an exponential decay function with a decay = T_1 .

A. cw-ODMR: The ODMR spectrum of NV^- centers is measured by alternating the microwave (MW) power between OFF and ON states. In the OFF state, NV^- centers are continuously (10-

100 ms pulses) pumped into the bright $|0\rangle$ state, while in the ON state, fluorescence is reduced as spins are driven into $|\mp 1\rangle$ states through the intersystem crossing to metastable singlet states [1]. The normalized fluorescence intensity is recorded as a function of the MW frequency at the applied magnetic field oriented along $[111]$ direction of the (100) diamond substrate (**Fig. 3a**). The resonance full-width-at-half-maximum linewidth Γ is 8.6 MHz, similar to the ensemble NV^- centers created by ^{14}N substitution [36]. The applied magnetic field breaks the degeneracy of the $|\mp 1\rangle$ state and leads to a pair of transitions for each NV^- orientation whose frequencies depend on the field projection along the NV symmetry axis. There are four sub-ensembles of NV centers with different symmetry axes; thus, a full ODMR spectrum contains 8 peaks (4 for $|0 \leftrightarrow 1\rangle$ transition and 4 for $|0 \leftrightarrow -1\rangle$ transition) [57]. To estimate the DC magnetic field sensitivity, we acquired the high-field ($|0 \leftrightarrow 1\rangle$) cw-ODMR spectrum at an applied field of 2.3 mT with optimized measurement parameters such as the laser power and MW power (inset of **Fig. 3a**) [45]. The minimum detected DC magnetic field within the shot noise is given by [14,25,58]: $\eta_{\text{CW}} \cong 4 \Gamma (3\sqrt{3} \gamma_{\text{NV}} C)^{-1} (R)^{-1/2}$, where $\gamma_{\text{NV}} = 28 \text{ GHz/T}$ is the gyromagnetic ratio of the electron spin, C is the ODMR peak contrast, R is the NV photon-detection rate. By using the parameters of the measurements (inset of **Fig. 3a**, $R = 200 \text{ mV} = 400 \text{ M counts/s}$ measured by using Thorlabs APD (APD440A) at laser power of 20 mW, $\Gamma = 8.6 \text{ MHz}$, $C = 0.1123$) we estimate a DC sensitivity of $\sim 104 \text{ nT/Hz}^{1/2}$ over $0.2 \mu\text{m}^3$ active volume.

- B. Rabi Nutation:** We performed Rabi nutation measurements to check the $T_{2,\text{Rabi}}$ decay [45] and know the π pulse length required to measure NV^- spin coherence lifetimes T_2 and T_1 of the plasma created NV^- centers (see below). We applied an MW frequency of 2629 MHz at the $|0 \leftrightarrow -1\rangle$ peak along $[111]$ orientation (the left ODMR peak in **Fig. 3a**) and recorded the NV fluorescence intensity vs the MW duration time t . **Fig. 3b** displays the measured Rabi oscillations fitted with a function $\sin(\omega_{\text{Rabi}} t) \exp(-t/T_{2,\text{Rabi}})$ (ω_{Rabi} is the Rabi frequency $\sim 4 \text{ MHz}$). The π pulse is 124 ns and $T_{2,\text{Rabi}}$ decay is $1.74 \mu\text{s}$ that can be extended to $> 50 \mu\text{s}$ upon a periodic reversal of the π phase [59].
- C. Transverse spin relaxation time (T_2):** Sensing weak dynamic (magnetic, electrical, or thermal) signals requires both high density of NV^- centers and longer T_2 relaxation times. We used a standard three-pulse Hahn-echo protocol to measure the T_2 of the Ar^+ plasma created NV^- centers [11,14,15]. The pulse sequence consists of a $\frac{\pi}{2} - \tau - \pi - \tau - \frac{\pi}{2}$ applied on the ODMR resonance peak at 2629 MHz in **Fig. 3a**, and the integrated NV fluorescence intensity is recorded as a function of the total evolution time 2τ (τ is the time between $\pi/2$ and π pulses). **Fig. 3c** shows a fast exponential decay of the Hahn-echo envelope ($4 \mu\text{s}$), explained by the strong dipolar interactions between the NV^- s and N paramagnetic centers (1 ppm in our CVD diamond). The contribution of ^{13}C spins in the NV echo signal at an applied magnetic field of 8.6 mT is negligible since the signal decays before the first ^{13}C revival ($20 \mu\text{s}$). The estimated sensitivity for dynamic (AC) magnetic fields is [25]: $\eta_{\text{AC}} \cong (\gamma_{\text{NV}} D)^{-1} 1 / (R T_{\text{meas}})^{1/2} \text{Exp}(T/T_2)$. T is the full field interrogation time, D is the spin echo contrast, and T_{meas} is the measurement averaging time. By using the parameters of our measurements ($T_2 = 4 \mu\text{s}$, $R = 200 \text{ mV} = 400 \text{ M counts/s}$, $D = 0.02$, $T_{\text{meas}} = 1 \text{ s}$, $T = 2 \mu\text{s}$) the sensitivity to AC magnetic fields is $0.12 \text{ pT Hz}^{-1/2}$. By using dynamical decoupling pulse sequence [25,31,41,60] T_2 can be extended to $> 100 \mu\text{s}$ for NV^- ensemble spins, and the AC sensitivity can be pushed to a few fT $\text{Hz}^{-1/2}$ [61].

D. Longitudinal spin relaxation time (T_1): We measured the longitudinal spin relaxation time (T_1) of the Ar^+ plasma-created NV^- centers using standard T_1 measurements [15,62]. We applied a sequence consisting of two laser pulses for NV initialization/readout ($10\ \mu\text{s}$ & $0.3\ \mu\text{s}$ in duration) with and without π pulse and recorded the subtracted fluorescence intensity as a function of the time t between the initialization and readout pulses. We plot the result of the T_1 measurements in **Fig. 3d** and found a $T_1 \sim 5\ \text{ms}$, similar to the values measured in CVD and EL diamonds. T_1 measurements are useful when using spin-correlation pulse protocols to bypass T_2 and improve AC sensitivity [15,31].

IV. Applications

High densities of NV^- s are favored for precision magnetometry due to improved signal-to-noise and sensitivity from $1/\sqrt{N}$ enhancement [25]. High densities also provide high fluorescence intensity, which can be measured by regular cheap photodetectors reducing the complexity of using SPCMs. To demonstrate magnetic field sensing applicability using the Ar^+ plasma-created NV^- centers, we implemented a magnetic field tracking method described by Welter *et al.* [17]. A 0.15 mT oscillatory magnetic field of various frequencies is applied to the NV^- sensors, which track the changes in the applied magnetic field in real-time, as shown in **Fig. 4**. We connected the tracking output voltage with an oscilloscope and recorded the time transient of the tracking signal along with applied magnetic field signals. As shown in **Fig. 4a**, the applied magnetic field changes 0.3 mT (peak-to-peak) over 20 ms time, and the tracking system can follow those changes in real-time. **Fig. 4b** shows the fast Fourier transform (FFT) of the measured tracking signals for all the applied oscillatory magnetic fields.

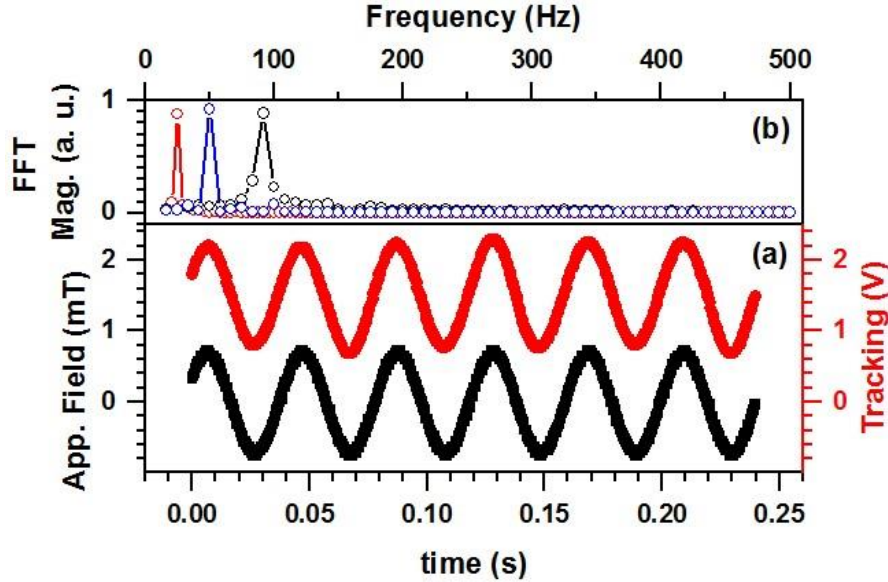


Figure 4. Real-time magnetic field measured using the NV^- centers created by high-energy photons from Ar^+ plasma over an active volume of $0.2\ \mu\text{m}^3$.

V. Conclusion

In summary, we demonstrated a low-cost and highly efficient method to create high-density NV^- centers on CVD-diamond crystal containing as-grown nitrogen concentrations of 1 ppm. The

measurements show that the high-density NV^- layer is distributed over 150-200 μm from the surface facing the photons created by Ar^+ plasma. It demonstrates that the described process creates an NV^- density of 0.57 ppm, yielding more than 50% N-to- NV^- conversion. We measured a DC magnetic field sensitivity of $\sim 104 \text{ nT Hz}^{-1/2}$ and an AC magnetic sensitivity of $\sim 0.12 \text{ pT Hz}^{-1/2}$ measured over $0.2 \mu\text{m}^3$ active sample volume. The measured relaxation properties are $T_1 = 5 \text{ ms}$ and $T_2 = 4 \mu\text{s}$. We found that the fluorescence intensity from the NV^- centers within $0.2 \mu\text{m}^3$ volume is detectable using regular photodetectors (e.g., APD), which is beneficial for on-chip and commercial adaptation [27]. The measurements show that using the Ar^+ plasma-created high-density NV^- can be used to measure magnetic fields quickly and efficiently at a rate over 10 mT/s with an active sample volume of $0.2 \mu\text{m}^3$. Our methodology could find applications in magnetometry where thick NV layers (150-200 μm) are needed to measure magnetic fields generated from big cells labeled with magnetic nanoparticles [63] or planetary bodies for paleomagnetic analysis of complex rocks such as meteorites that have heterogeneous magnetizations $\leq 200 \mu\text{m}$ [64].

VI. Acknowledgments

K.A. would like to acknowledge the support of the National Science Foundation/EPSCoR RII Track-4 Award OIA-2033210. The research was partially performed in the Nebraska Nanoscale Facility, which is supported by the National Science Foundation under Award ECCS: 2025298 and the Nebraska Research Initiative. P.B.K. would like to acknowledge the support of the Wichita State University Convergence Science Initiative Program. A. L. would like to acknowledge the support of the National Science Foundation/EPSCoR RII Track-1: Emergent Quantum Materials and Technologies (EQUATE), Award OIA-2044049.

VII. AUTHOR DECLARATIONS

a. Conflict of Interest

The authors have no conflicts to disclose.

b. Author Contributions

K.A. conceived the experiment and supervised the overall study. P.B.K., R.T., M.D., A.L., and K.A. performed the measurements and analyzed the data. A. E. A. helped in data analysis and figure preparation for the manuscript. A.L. and K.A. wrote the manuscript with help from all authors. P.B.K. and R.T. contribute equally.

VIII. DATA AVAILABILITY

The data supporting this study's findings are available from the corresponding author upon reasonable request.

References

- [1] M. W. Doherty, N. B. Manson, P. Delaney, F. Jelezko, J. Wrachtrup, and L. C. L. Hollenberg, *The Nitrogen-Vacancy Colour Centre in Diamond*, Physics Reports **528**, 1 (2013).
- [2] N. Y. Yao, L. Jiang, A. V. Gorshkov, P. C. Maurer, G. Giedke, J. I. Cirac, and M. D. Lukin, *Scalable Architecture for a Room Temperature Solid-State Quantum Information Processor*, Nat Commun **3**, 800 (2012).
- [3] T. van der Sar, Z. H. Wang, M. S. Blok, H. Bernien, T. H. Taminiau, D. M. Toyli, D. A. Lidar, D. D. Awschalom, R. Hanson, and V. V. Dobrovitski, *Decoherence-Protected Quantum Gates for a Hybrid Solid-State Spin Register*, Nature **484**, 82 (2012).
- [4] S. Prawer and I. Aharonovich, *Quantum Information Processing with Diamond: Principles and Applications*, 1st ed. (Woodhead Publishing, Limited, 2018).
- [5] H. Bernien et al., *Heralded Entanglement between Solid-State Qubits Separated by Three Metres*, Nature **497**, 86 (2013).
- [6] G. D. Fuchs, G. Burkard, P. V. Klimov, and D. D. Awschalom, *A Quantum Memory Intrinsic to Single Nitrogen–Vacancy Centres in Diamond*, Nature Phys **7**, 789 (2011).
- [7] C. E. Bradley, J. Randall, M. H. Abobeih, R. C. Berrevoets, M. J. Degen, M. A. Bakker, M. Markham, D. J. Twitchen, and T. H. Taminiau, *A Ten-Qubit Solid-State Spin Register with Quantum Memory up to One Minute*, Phys. Rev. X **9**, 031045 (2019).
- [8] Y.-Y. Lai, G.-D. Lin, J. Twamley, and H.-S. Goan, *Single-Nitrogen-Vacancy-Center Quantum Memory for a Superconducting Flux Qubit Mediated by a Ferromagnet*, Phys. Rev. A **97**, 052303 (2018).
- [9] C. L. Degen, F. Reinhard, and P. Cappellaro, *Quantum Sensing*, Rev. Mod. Phys. **89**, 035002 (2017).
- [10] F. Casola, T. van der Sar, and A. Yacoby, *Probing Condensed Matter Physics with Magnetometry Based on Nitrogen-Vacancy Centres in Diamond*, Nat Rev Mater **3**, 1 (2018).
- [11] J. R. Maze et al., *Nanoscale Magnetic Sensing with an Individual Electronic Spin in Diamond*, Nature **455**, 644 (2008).
- [12] R. Schirhagl, K. Chang, M. Loretz, and C. L. Degen, *Nitrogen-Vacancy Centers in Diamond: Nanoscale Sensors for Physics and Biology*, Annu. Rev. Phys. Chem. **65**, 83 (2014).
- [13] A. Laraoui, J. S. Hodges, C. A. Ryan, and C. A. Meriles, *Diamond Nitrogen-Vacancy Center as a Probe of Random Fluctuations in a Nuclear Spin Ensemble*, Phys. Rev. B **84**, 104301 (2011).
- [14] A. Laraoui, J. S. Hodges, and C. A. Meriles, *Magnetometry of Random Ac Magnetic Fields Using a Single Nitrogen-Vacancy Center*, Appl. Phys. Lett. **97**, 143104 (2010).
- [15] A. Laraoui, F. Dolde, C. Burk, F. Reinhard, J. Wrachtrup, and C. A. Meriles, *High-Resolution Correlation Spectroscopy of ^{13}C Spins near a Nitrogen-Vacancy Centre in Diamond*, Nat Commun **4**, 1651 (2013).
- [16] A. Laraoui and K. Ambal, *Opportunities for Nitrogen-Vacancy-Assisted Magnetometry to Study Magnetism in 2D van Der Waals Magnets*, Appl. Phys. Lett. **121**, 060502 (2022).
- [17] P. Welter, B. A. Josteinsson, S. Josephy, A. Wittmann, A. Morales, G. Puebla-Hellmann, and C. L. Degen, *Fast Scanning Nitrogen-Vacancy Magnetometry by Spectrum Demodulation*, (2022).
- [18] F. Dolde et al., *Electric-Field Sensing Using Single Diamond Spins*, Nature Phys **7**, 459 (2011).

- [19] M. S. J. Barson, L. M. Oberg, L. P. McGuinness, A. Denisenko, N. B. Manson, J. Wrachtrup, and M. W. Doherty, *Nanoscale Vector Electric Field Imaging Using a Single Electron Spin*, Nano Lett. **21**, 2962 (2021).
- [20] M. Block et al., *Optically Enhanced Electric Field Sensing Using Nitrogen-Vacancy Ensembles*, Phys. Rev. Appl. **16**, 024024 (2021).
- [21] J. Michl et al., *Robust and Accurate Electric Field Sensing with Solid State Spin Ensembles*, Nano Lett. **19**, 4904 (2019).
- [22] G. Kucsko, P. C. Maurer, N. Y. Yao, M. Kubo, H. J. Noh, P. K. Lo, H. Park, and M. D. Lukin, *Nanometre-Scale Thermometry in a Living Cell*, Nature **500**, 54 (2013).
- [23] A. Laraoui, H. Aycok-Rizzo, Y. Gao, X. Lu, E. Riedo, and C. A. Meriles, *Imaging Thermal Conductivity with Nanoscale Resolution Using a Scanning Spin Probe*, Nat Commun **6**, 8954 (2015).
- [24] M. Fujiwara et al., *Real-Time Nanodiamond Thermometry Probing in Vivo Thermogenic Responses*, Sci. Adv. **6**, eaba9636 (2020).
- [25] J. F. Barry, J. M. Schloss, E. Bauch, M. J. Turner, C. A. Hart, L. M. Pham, and R. L. Walsworth, *Sensitivity Optimization for NV-Diamond Magnetometry*, Rev. Mod. Phys. **92**, 015004 (2020).
- [26] D. Budker and M. Romalis, *Optical Magnetometry*, Nature Phys **3**, 4 (2007).
- [27] D. Kim, M. I. Ibrahim, C. Foy, M. E. Trusheim, R. Han, and D. R. Englund, *A CMOS-Integrated Quantum Sensor Based on Nitrogen–Vacancy Centres*, Nat Electron **2**, 284 (2019).
- [28] V. M. Acosta et al., *Diamonds with a High Density of Nitrogen-Vacancy Centers for Magnetometry Applications*, Phys. Rev. B **80**, 115202 (2009).
- [29] T. Staudacher, F. Ziem, L. Häussler, R. Stöhr, S. Steinert, F. Reinhard, J. Scharpf, A. Denisenko, and J. Wrachtrup, *Enhancing the Spin Properties of Shallow Implanted Nitrogen Vacancy Centers in Diamond by Epitaxial Overgrowth*, Appl. Phys. Lett. **101**, 212401 (2012).
- [30] F. Feng, W. Zhang, J. Zhang, L. Lou, W. Zhu, and G. Wang, *Optimizing the Density of Nitrogen Implantation for Generating High-Density NV Center Ensembles for Quantum Sensing*, Eur. Phys. J. D **73**, 202 (2019).
- [31] P. Kehayias et al., *Solution Nuclear Magnetic Resonance Spectroscopy on a Nanostructured Diamond Chip*, Nat Commun **8**, 188 (2017).
- [32] E. E. Kleinsasser, M. M. Stanfield, J. K. Q. Banks, Z. Zhu, W.-D. Li, V. M. Acosta, H. Watanabe, K. M. Itoh, and K.-M. C. Fu, *High Density Nitrogen-Vacancy Sensing Surface Created via He+ Ion Implantation of 12C Diamond*, Appl. Phys. Lett. **108**, 202401 (2016).
- [33] I. Fescenko, A. Laraoui, J. Smits, N. Mosavian, P. Kehayias, J. Seto, L. Bougas, A. Jarmola, and V. M. Acosta, *Diamond Magnetic Microscopy of Malarial Hemozoin Nanocrystals*, Phys. Rev. Appl. **11**, 034029 (2019).
- [34] M. Capelli, A. H. Heffernan, T. Ohshima, H. Abe, J. Jeske, A. Hope, A. D. Greentree, P. Reineck, and B. C. Gibson, *Increased Nitrogen-Vacancy Centre Creation Yield in Diamond through Electron Beam Irradiation at High Temperature*, Carbon **143**, 714 (2019).
- [35] S. V. Bolshedvorskii et al., *The Study of the Efficiency of Nitrogen to Nitrogen-Vacancy (NV)-Center Conversion in High-Nitrogen Content Samples*, Physica Rapid Research Ltrs **2200415** (2023).
- [36] G. de Lange, T. van der Sar, M. Blok, Z.-H. Wang, V. Dobrovitski, and R. Hanson, *Controlling the Quantum Dynamics of a Mesoscopic Spin Bath in Diamond*, Sci Rep **2**, 382 (2012).

- [37] A. Laraoui, J. S. Hodges, and C. A. Meriles, *Nitrogen-Vacancy-Assisted Magnetometry of Paramagnetic Centers in an Individual Diamond Nanocrystal*, Nano Lett. **12**, 3477 (2012).
- [38] H. Park, J. Lee, S. Han, S. Oh, and H. Seo, *Decoherence of Nitrogen-Vacancy Spin Ensembles in a Nitrogen Electron-Nuclear Spin Bath in Diamond*, Npj Quantum Inf **8**, 1 (2022).
- [39] B. Campbell, W. Choudhury, A. Mainwood, M. Newton, and G. Davies, *Lattice Damage Caused by the Irradiation of Diamond*, Nuclear Instruments and Methods in Physics Research Section A: Accelerators, Spectrometers, Detectors and Associated Equipment **476**, 680 (2002).
- [40] L. Băni et al., *A Study of the Radiation Tolerance of Poly-Crystalline and Single-Crystalline CVD Diamond to 800 MeV and 24 GeV Protons*, J. Phys. D: Appl. Phys. **52**, 465103 (2019).
- [41] J. Smits, J. T. Damron, P. Kehayias, A. F. McDowell, N. Mosavian, I. Fescenko, N. Ristoff, A. Laraoui, A. Jarmola, and V. M. Acosta, *Two-Dimensional Nuclear Magnetic Resonance Spectroscopy with a Microfluidic Diamond Quantum Sensor*, Sci. Adv. **5**, eaaw7895 (2019).
- [42] B. Grotz et al., *Charge State Manipulation of Qubits in Diamond*, Nat Commun **3**, 729 (2012).
- [43] H. Jayakumar, J. Henshaw, S. Dhomkar, D. Pagliero, A. Laraoui, N. B. Manson, R. Albu, M. W. Doherty, and C. A. Meriles, *Optical Patterning of Trapped Charge in Nitrogen-Doped Diamond*, Nat Commun **7**, 12660 (2016).
- [44] K. J. Brown, E. Chartier, E. M. Sweet, D. A. Hopper, and L. C. Bassett, *Cleaning Diamond Surfaces Using Boiling Acid Treatment in a Standard Laboratory Chemical Hood*, J. Chem. Health Saf. **26**, 40 (2019).
- [45] S. v. Bolshedvorskii et al., *The Study of the Efficiency of Nitrogen to NV-Center Conversion in High Nitrogen Content Samples*, Physica Status Solidi (RRL) – Rapid Research Letters **n/a**, (n.d.).
- [46] S. A. Bogdanov, A. M. Gorbachev, D. B. Radishev, A. L. Vikharev, M. A. Lobaev, S. A. Gusev, D. A. Tatarsky, S. V. Bolshedvorskii, A. V. Akimov, and V. V. Chernov, *Creation of Localized NV Center Ensembles in CVD Diamond by Electron Beam Irradiation*, Tech. Phys. Lett. **45**, 281 (2019).
- [47] K. Ambal, A. Payne, D. P. Waters, C. C. Williams, and C. Boehme, *Spin-Relaxation Dynamics of E' Centers at High Density in SiO₂ Thin Films for Single-Spin Tunneling Force Microscopy*, Phys. Rev. Applied **4**, 024008 (2015).
- [48] Y. Ishikawa, M. Okigawa, S. Samukawa, and S. Yamasaki, *Reduction of Plasma-Induced Damage in SiO₂ Films during Pulse-Time-Modulated Plasma Irradiation*, Journal of Vacuum Science & Technology B: Microelectronics and Nanometer Structures Processing, Measurement, and Phenomena **23**, 389 (2005).
- [49] Y. Ichihashi, Y. Ishikawa, Y. Kato, R. Shimizu, M. Okigawa, and S. Samukawa, *Effects of Thermal Annealing for Restoration of UV Irradiation Damage during Plasma Etching Processes*, Jpn. J. Appl. Phys. **45**, 8370 (2006).
- [50] S. Espinho, E. Felizardo, J. Henriques, and E. Tatarova, *Vacuum Ultraviolet Radiation Emitted by Microwave Driven Argon Plasmas*, Journal of Applied Physics **121**, 153303 (2017).
- [51] F. Lebreton, S. N. Abolmasov, F. Silva, and P. R. i Cabarrocas, *In Situ Photoluminescence Study of Plasma-Induced Damage at the a-Si:H/c-Si Interface*, Applied Physics Letters **108**, 051603 (2016).
- [52] A. Kramida, Y. Ralchenko, J. Reader, and NIST ASD Team, *NIST Atomic Spectra Database (Ver. 5.10)*, National Institute of Standards and Technology, Gaithersburg, MD (n.d.).
- [53] S. Samukawa et al., *The 2012 Plasma Roadmap*, J. Phys. D: Appl. Phys. **45**, 253001 (2012).

- [54] C. X. Li, Q. Y. Zhang, N. Zhou, B. C. Hu, C. Y. Ma, C. Zhang, and Z. Yi, *UV-Induced Charge-State Conversion from the Negatively to Neutrally Charged Nitrogen-Vacancy Centers in Diamond*, Journal of Applied Physics **132**, 215102 (2022).
- [55] A. Erickson, S. Q. A. Shah, A. Mahmood, I. Fescenko, R. Timalisina, C. Binek, and A. Laraoui, *Nanoscale Imaging of Antiferromagnetic Domains in Epitaxial Films of Cr₂O₃ via Scanning Diamond Magnetic Probe Microscopy*, RSC Advances **13**, 178 (2023).
- [56] A. Laraoui and C. A. Meriles, *Approach to Dark Spin Cooling in a Diamond Nanocrystal*, ACS Nano **7**, 3403 (2013).
- [57] Y. Matsuzaki, H. Morishita, T. Shimooka, T. Tashima, K. Kakuyanagi, K. Semba, W. J. Munro, H. Yamaguchi, N. Mizuochi, and S. Saito, *Optically Detected Magnetic Resonance of High-Density Ensemble of NV⁻ Centers in Diamond*, J. Phys.: Condens. Matter **28**, 275302 (2016).
- [58] A. Dréau, M. Lesik, L. Rondin, P. Spinicelli, O. Arcizet, J.-F. Roch, and V. Jacques, *Avoiding Power Broadening in Optically Detected Magnetic Resonance of Single NV Defects for Enhanced Dc Magnetic Field Sensitivity*, Phys. Rev. B **84**, 195204 (2011).
- [59] A. Laraoui and C. A. Meriles, *Rotating Frame Spin Dynamics of a Nitrogen-Vacancy Center in a Diamond Nanocrystal*, Phys. Rev. B **84**, 161403 (2011).
- [60] L. M. Pham, N. Bar-Gill, C. Belthangady, D. Le Sage, P. Cappellaro, M. D. Lukin, A. Yacoby, and R. L. Walsworth, *Enhanced Solid-State Multispin Metrology Using Dynamical Decoupling*, Phys. Rev. B **86**, 045214 (2012).
- [61] Y. Xie, H. Yu, Y. Zhu, X. Qin, X. Rong, C.-K. Duan, and J. Du, *A Hybrid Magnetometer towards Femtotesla Sensitivity under Ambient Conditions*, Science Bulletin **66**, 127 (2021).
- [62] A. Jarmola, V. M. Acosta, K. Jensen, S. Chemerisov, and D. Budker, *Temperature- and Magnetic-Field-Dependent Longitudinal Spin Relaxation in Nitrogen-Vacancy Ensembles in Diamond*, Phys. Rev. Lett. **108**, 197601 (2012).
- [63] D. R. Glenn, K. Lee, H. Park, R. Weissleder, A. Yacoby, M. D. Lukin, H. Lee, R. L. Walsworth, and C. B. Connolly, *Single-Cell Magnetic Imaging Using a Quantum Diamond Microscope*, Nat Methods **12**, 736 (2015).
- [64] R. R. Fu, E. A. Lima, M. W. R. Volk, and R. Trubko, *High-Sensitivity Moment Magnetometry With the Quantum Diamond Microscope*, Geochem Geophys Geosyst **21**, (2020).